A myopathy-linked tropomyosin mutation severely alters thin filament conformational changes during activation

Julien Ochala[a,1], Hiroyuki Iwamoto[b], Lars Larsson[a,c], and Naoto Yagi[b]

[a]Department of Neuroscience, Clinical Neurophysiology, Uppsala University, 751 85 Uppsala, Sweden; [b]Japan Synchrotron Radiation Research Institute, Sayo-cho, Sayo-gun, Hyogo 679-6198, Japan; and [c]Department of Biobehavioral Health, Pennsylvania State University, University Park, PA 16802

Edited by Clara Franzini-Armstrong, University of Pennsylvania Medical Center, Philadelphia, PA, and approved April 23, 2010 (received for review February 12, 2010)

Human point mutations in β- and γ-tropomyosin induce contractile deregulation, skeletal muscle weakness, and congenital myopathies. The aim of the present study was to elucidate the hitherto unknown underlying molecular mechanisms. Hence, we recorded and analyzed the X-ray diffraction patterns of human membrane-permeabilized muscle cells expressing a particular β-tropomyosin mutation (R133W) associated with a loss in cell force production, in vivo muscle weakness, and distal arthrogryposis. Upon addition of calcium, we notably observed less intensified changes, compared with controls, (*i*) in the second (1/19 nm^{-1}), sixth (1/5.9 nm^{-1}), and seventh (1/5.1 nm^{-1}) actin layer lines of cells set at a sarcomere length, allowing an optimal thin-thick filament overlap; and (*ii*) in the second actin layer line of overstretched cells. Collectively, these results directly prove that during activation, switching of a positive to a neutral charge at position 133 in the protein partially hinders both calcium- and myosin-induced tropomyosin movement over the thin filament, blocking actin conformational changes and consequently decreasing the number of cross-bridges and subsequent force production.

actin | cross-bridge | single-muscle fiber | X-ray diffraction

Tropomyosin is expressed in multiple isoforms in most mammalian cell types (1, 2). The isoform diversity is related to alternative splicing, alternative promoters, and differential RNA processing, resulting in specific striated muscle, smooth muscle, and nonmuscle isoforms (2). In skeletal muscle there are three major isoforms, α, β, and γ, which are encoded by the *TPM1*, *TPM2*, and *TPM3* genes, respectively (2). A number of missense defects in these *TPM2* and *TPM3* genes cause single amino acid changes in β- and γ-tropomyosin, skeletal muscle weakness, and myopathies (3). The molecular mechanisms by which such subtle defects result in muscle contractile dysfunction remain unclear and need to be elucidated with the aim of targeting potential therapies.

A unique β-tropomyosin mutation (R133W) resulting from a defect in the *TPM2* gene was recently identified in patients with distal arthrogryposis and an autosomal dominant congenital myopathy (4). These patients suffered from generalized weakness in both proximal and distal muscles. Biopsy specimens did not reveal any signs of atrophy or other histopathological abnormalities (4). Nevertheless, in normal-sized fibers, cell-physiological experiments disclosed a large decrease in maximal isometric force production (Fig. 1) as well as changes in kinetics: that is, a slower rate of force development and a faster maximum unloaded shortening velocity (5), implying a slower rate of motor protein myosin attachment and a faster rate of detachment from actin monomers. This finding suggests a reduced number of cross-bridges in the strong binding state, resulting in overall weakness in the patients (5). How does the R133W mutation induce such dysfunction? To date, at the molecular level no experimentally-based explanation exists.

In skeletal muscle, tropomyosin is an integral component of the sarcomere, and during contraction its movement, as well as the movements of the other thin filament structures, are controlled by calcium and myosin (6, 7). Hence, we hypothesize that the R133W mutation perturbs the calcium- and myosin-related thin-filament displacements leading to the myopathic phenotype. In the present study the primary aim was to test this hypothesis by recording and analyzing X-ray diffraction patterns. A secondary goal was to distinguish between calcium- and myosin-induced changes in thin-filament movements. Thus, we compared membrane-permeabilized skeletal muscle cells from patients carrying the R133W β-tropomyosin defect with corresponding cells from healthy controls. We monitored the tropomyosin [the far off-meridional part of the second actin layer line (ALL) at 1/19 nm^{-1}] and actin (sixth and seventh ALL at 1/5.9 and 1/5.1 nm^{-1}, respectively) intensity changes during activation under various conditions. The results first emphasized that upon addition of calcium, at an optimal sarcomere length, the second, sixth, and seventh ALL reflections were less intensified in fibers carrying the β-tropomyosin mutation. Thus, tropomyosin movement over the thin filament was partially inhibited, hindering the activation-induced actin conformational changes. Second, it was evident that the second ALL intensity change was also attenuated in overstretched cells, indicating that calcium- and myosin-related thin-filament movements are both affected by the single amino acid modification in the protein coded by the *TPM2* gene.

Results

X-ray recordings of human muscle were successfully achieved. The diffraction patterns in preactivating/activating and low-EGTA rigor/calcium-rigor solutions are shown in Figs. 2 *A*, *B*, *D*, and *E* and 3 *A*, *B*, *D*, and *E*. All intensities are summarized in Tables 1 and 2.

In control membrane-permeabilized cells set at a sarcomere length considered as optimal (2.70 μm), where there is a full thin-thick filament overlap, the second ALL (1/19 nm^{-1}) appeared in red (Fig. 2*C*), indicating that the reflection was enhanced upon addition of calcium. The sixth (1/5.9 nm^{-1}) and seventh (1/5.1 nm^{-1}) ALLs were also intensified (Fig. 2*C*). This finding corroborates previous data obtained in frogs and rabbits (8–10). In fibers carrying the R133W β-tropomyosin mutation, with the same sarcomere length, the reflections of the second and sixth ALLs were also enhanced during activation, but to a lesser extent when compared with controls (Fig. 2*F*). The intensity of the seventh ALL was, however, unaffected by activation.

A separate number of cells were overstretched beyond the thin-thick filament overlap (sarcomere length > 3.60 μm). In the

Author contributions: J.O., H.I., L.L., and N.Y. designed research; J.O., H.I., and N.Y. performed research; J.O. and H.I. contributed new reagents/analytic tools; J.O. and H.I. analyzed data; and J.O., H.I., L.L., and N.Y. wrote the paper.

The authors declare no conflict of interest.

This article is a PNAS Direct Submission.

[1]To whom correspondence should be addressed. E-mail: julien.ochala@neuro.uu.se.

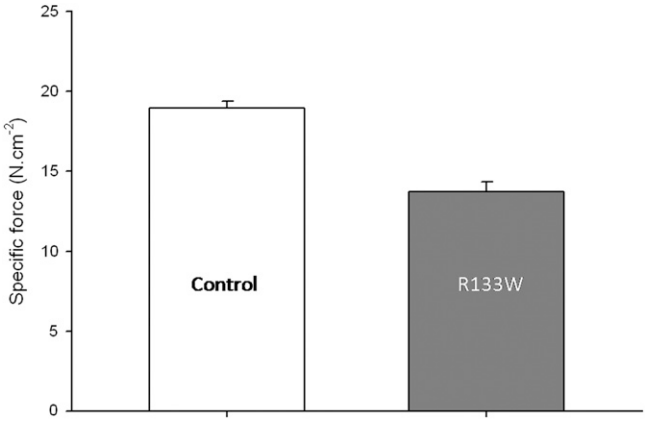

Fig. 1. Specific force of membrane-permeabilized muscle cells from controls (CTL) and patients (R133W), corresponding to maximal isometric force production normalized to cell cross-sectional area. Values of fibers expressing the type I and IIa myosin heavy-chain isoforms are pooled together, as they did not differ significantly. These values have already been published elsewhere (5) and are given here as means ± SEs.

low-EGTA rigor solution, the second ALL reflection in controls was higher than that at optimal sarcomere length in a similar solution. This result may have been because of substantial inhomogeneities in sarcomere length, provoking a possible residual thin-thick filament overlap, with consequent rigor cross-bridge formation. On addition of calcium, in the calcium-rigor solution, the second ALL reflection of controls was increased (Fig. 3*C*), whereas the sixth ALL had shifted slightly outward and its intensity was slightly decreased (Fig. 3*C*). These observations differ from the previous finding, in overstretched cells from frogs and rabbits, in which the sixth ALL reflection was slightly enhanced without any shift of its peak position (10, 11). As mentioned above, this discrepancy may have been because of some remaining rigor cross-bridges. In fact, in the absence of calcium, these rigor cross-bridges may enhance the inner part of the sixth ALL and, later during activation, may slowly detach from actin, resulting in an outward shift of the reflection as well as a decrease in the intensity. The seventh ALL intensity was unaffected (Fig. 3*C*). In fibers expressing the R133W β-tropomyosin mutation, weaker enhancement of the second ALL reflection was observed on addition of calcium, in comparison with control cells (Fig. 3*F*). On the other hand, the intensities of the sixth and seventh ALLs did not differ from those of the controls and were lightly decreased or unchanged, respectively (Fig. 3*F*).

Equatorial reflections (1,0 and 1,1 intensities) were analyzed and the ratio of $I_{1,1}$ to $I_{1,0}$ was calculated for fibers set at the optimal sarcomere length (2.70 μm). In control fibers, this ratio increased upon addition of calcium, confirming other findings (12). In cells expressing the R133W β-tropomyosin mutation, a weaker augmentation was observed when compared with controls.

In addition to X-ray recordings, the slack-test procedure was applied to a separate number of membrane-permeabilized muscle fibers. All control fibers displayed a monophasic shortening during the procedure. In fact, straight lines were observed between the release length change and the time taken to redevelop force. The slopes of these lines divided by the fiber length were defined as maximum unloaded shortening velocity (V_0). Mean V_0 was 0.83 (± 0.04) ML.s^{-1} (muscle length per second). On the other hand, all cells carrying the R133W β-tropomyosin mutation exhibited a biphasic shortening during the slack-test, which consisted of two distinct linear phases (Fig. 4) characterized by an initial fast phase of shortening and a second, slower phase with an apparent break point at ≈13% of length change. The slopes of these two lines divided by the fiber length were termed V_{01} and V_{02}, respectively. Mean V_{01} was 1.11 ± 0.03 ML.s^{-1} and mean V_{02} was 0.30 ± 0.06 ML.s^{-1}. Such biphasic shortening behavior occurs at a nonsaturating calcium concentration in normal cells (13) or during maximal activation in fibers from which troponin C has been partially removed (14). The first, fast phase is thought to be calcium-insensitive, whereas the second, slower part is dependent on the calcium concentration and subsequent thin filament activation-deactivation (13, 15).

Discussion

With the aim of identifying the molecular mechanisms by which a single amino acid change (R133W) in β-tropomyosin induces muscle weakness, X-ray diffraction patterns of membrane-permeabilized cells carrying this specific defect were recorded, analyzed, and compared with human control muscle fibers. Upon addition of calcium, weaker intensity changes were noted (*i*) in the second, sixth, and seventh ALLs of fibers set at a sarcomere length allowing an optimal thin-thick filament overlap; and (*ii*) in the second ALL of overstretched cells.

The second ALL is one of the most documented reflections in vertebrate muscle. During activation, its intensity change orig-

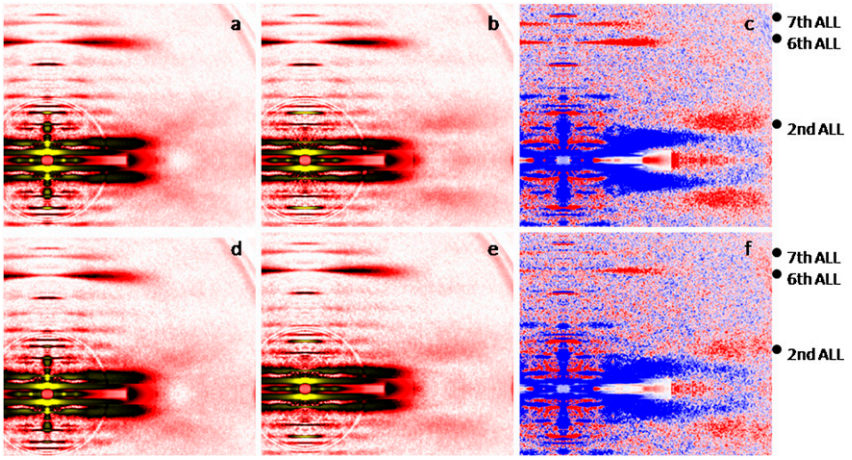

Fig. 2. X-ray diffraction patterns from human control (*A*–*C*) and mutated (*D*–*F*) cells set at an optimal sarcomere length, in preactivating (*A* and *D*) and activating (*B* and *E*) solutions. There are differences in intensity profiles (*C* and *F*); red and blue colors indicate the enhanced and weakened areas, respectively, after addition of calcium. ALL, actin layer line.

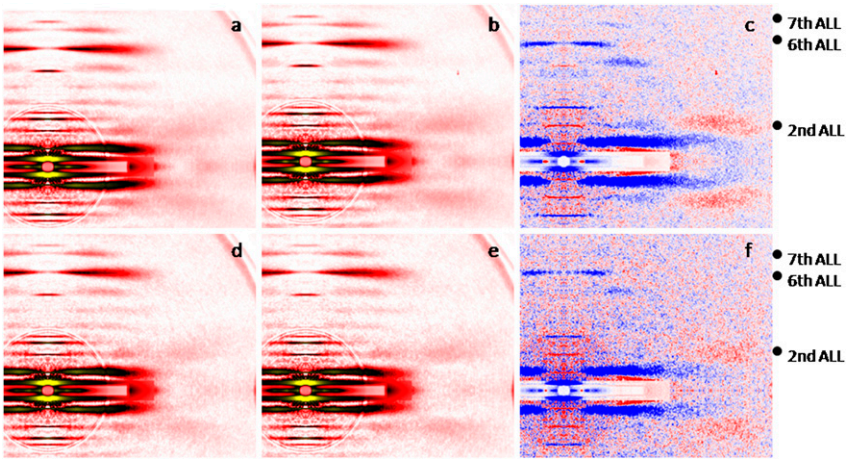

Fig. 3. X-ray diffraction patterns from human control (*A–C*) and mutated (*D–F*) overstretched fibers, in low-EGTA rigor (*A* and *D*) and calcium-rigor (*B* and *E*) solutions. There are differences in intensity profiles (*C* and *F*); red and blue colors indicate the enhanced and weakened areas, respectively, after addition of calcium.

inates from movement of tropomyosin over the thin filament, exposing myosin binding sites on actin that are essential for cross-bridge formation (16). Direct attachment of myosin to actin clearly does not contribute to this reflection modification, as that the motor protein is disordered during contraction (17). Here, the weaker intensity change of the second ALL of mutated cells set at a full thin-thick filament overlap proves that tropomyosin displacement over the surface of actin is partially hindered when compared with controls. In an attempt to identify the origin of such dysfunction (calcium- vs. myosin-related), fibers were overstretched to minimize thin-thick filament overlap (18). Upon addition of calcium, the second ALL intensity change of mutated cells was also smaller when compared with control fibers, demonstrating that calcium- and myosin-induced movements are both unspecifically altered. The underlying electrostatic mechanisms may be complex. The mutation is located in a highly conserved region (4) and theoretically may disrupt the coiled-coil dimeric structure of tropomyosin, as well as the affinity of tropomyosin for other thin filament proteins, such as actin. In fact, the replacement of the positively charged arginine by a neutral amino acid, tryptophan, in the "g" position of the heptad repeat, may disturb the specific interaction with the negatively charged glutamic acid in the "e" position of the opposing strand (Fig. 5) (19, 20). In addition, the crucial position of the mutation in the fourth of the seven tropomyosin pseudorepeats (residues 124–165) may directly affect the binding to actin amino acid residues (Fig. 5) (21). Thus, the locally modified stability and flexibility may impede tropomyosin movement in the presence of calcium, altering the normal equilibrium positions (22–26). Hence, fewer myosin binding sites will be exposed on actin and fewer cross-bridges in the strong binding state can be formed. This finding is further validated by the reduced ratio of $I_{1,1}$ to $I_{1,0}$. All of these findings are consistent with the dramatic reduction in maximal isometric force production (Fig. 1) and with the slower rate of force development of membrane-permeabilized fibers expressing the same mutation (5). On the other hand, the increase in unloaded shortening velocity (V_0) observed with the use of the slack-test procedure may need further explanation (5). In normal fibers, during rapid unloading, and at a saturating calcium concentration, the number of cross-bridges is markedly reduced, but not enough to provoke significant deactivation of the fully activated thin filament units, leading to a fast monophasic pattern (Fig. 4) (27). In cells with the R133W defect, this behavior differs; tropomyosin has not entirely moved and shortening-induced deactivation may occur, giving rise to two phases in the slack-test plot (Fig. 4), as previously shown at a nonsaturating calcium concentration in normal cells (13) and during maximal activation in fibers with partially removed troponin C (14). Thus, the occurrence of the second, slow phase (V_{02}) may arise from the partially inactive tropomyosin and other thin filament proteins (27), whereas the acceleration of the initial, fast phase (V_{01}) with the mutation may

Table 1. Integrated intensities of the major thin filament-based reflections in the recordings shown in Figs. 2 and 3

	Sarcomere length	Condition	Second ALL	Sixth ALL	Seventh ALL
Control	2.70 μm	Preactivation	0.047 ± 0.007	1	0.323 ± 0.015
		Activation	0.186 ± 0.009*	1.120 ± 0.028*	0.392 ± 0.031*
	3.60 μm	Preactivation	0.074 ± 0.005	1	0.252 ± 0.003
		Activation	0.150 ± 0.002*	0.946 ± 0.006*	0.236 ± 0.002
R133W	2.70 μm	Preactivation	0.059 ± 0.008	1	0.334 ± 0.012
		Activation	0.128 ± 0.008*†	1.025 ± 0.019*†	0.341 ± 0.016
	3.60 μm	Preactivation	0.077 ± 0.005	1	0.283 ± 0.011
		Activation	0.125 ± 0.007*†	0.952 ± 0.009*	0.272 ± 0.014

Values from activated fibers set at a full thin-thick filament overlap are normalized using the sixth ALL data from the same relaxed fibers. Similarly, data from overstretched activated cells are normalized using the sixth ALL data from the same overstretched cells in the absence of calcium. All values are means ± SE.
*Significant difference compared with preactivation for the same group (control or R133W).
†Significant difference compared with controls under the same condition (preactivation or activation).

Table 2. Integrated intensities of the equatorial reflections 1,0 and 1,1

	Sarcomere length	Condition	$I_{1,0}$	$I_{1,1}$	$I_{1,1}/I_{1,0}$
Control	2.70 μm	Preactivation	1.061 ± 0.045	0.676 ± 0.044	0.639 ± 0.036
		Activation	0.354 ± 0.027	0.529 ± 0.038	1.505 ± 0.073*
R133W	2.70 μm	Preactivation	0.801 ± 0.103	0.463 ± 0.064	0.607 ± 0.082
		Activation	0.301 ± 0.038	0.349 ± 0.051	1.160 ± 0.150*†

Because of the copper mask, the intensities should be multiplied by 7. Values from activated fibers set at a full thin-thick filament overlap are normalized using the sixth ALL data from the same relaxed fibers. Similarly, data from overstretched activated cells are normalized using the sixth ALL data from the same overstretched cells in the absence of calcium. All values are means ± SE.

*Significant difference compared with preactivation for the same group (control or R133W).

†Significant difference compared with controls under the same condition (preactivation or activation).

originate from a thin filament-linked increase in the rate of myosin detachment from actin monomers (5).

During activation, the sixth and seventh ALL reflections are known to increase in vertebrate muscle. These increases are likely to be caused by actin monomers modifying their molecular shape rather than by binding of myosin to the thin filament (28). Each actin monomer may undergo an axial compression via closing-ups between subdomains 1 and 2 and between subdomains 3 and 4 (29). In the present study, at an optimal thin-thick filament overlap, calcium-induced intensity changes in the sixth and seventh ALLs of mutated cells were greatly weakened when compared with controls, indicating that activation-induced actin conformational changes are almost nonexistent. Different potential alternatives may underlie this phenomenon. First, one may suggest that myosin attachment is one of the triggers for actin conformational changes in vertebrate muscle. In this regard, tropomyosin movement blockade over the thin filament—thus, over the surface of actin—would prevent cross-bridge formation and potential subsequent modifications in the actin structure. This alternative may be inappropriate in view of the extent to which the sixth and seventh ALL reflections are reduced when compared with the small decrease in the $I_{1,1}$ to $I_{1,0}$ ratio of mutated fibers. Second, a more likely mechanism may be proposed, where tropomyosin movement over the thin filament is directly responsible for actin conformational changes during activation in skeletal muscle. In such a case, the switching of a positive to a neutral charge at position 133 and the consequent incomplete tropomyosin displacement would lead to either a partial inhibition of every actin monomer or a full blockade of the actin monomers that are still "covered" by the inactive tropomyosin portion.

In conclusion, the present study directly unravels the molecular mechanisms underlying contractile dysfunction in cells expressing a particular R133W β-tropomyosin mutation. The results directly demonstrate that during activation, the single amino acid change in the protein partially inhibits both calcium- and myosin-induced tropomyosin movement over the thin filament, preventing actin conformational changes and thereby reducing the number of cross-bridges and the consequent force production. Thus, interventions that would primarily restore tropomyosin movement may represent potential therapeutic strategies for the future.

Materials and Methods

Subjects. The study was conducted on two patients with distal arthrogryposis type 2B, and carrying a R133W β-tropomyosin mutation (4, 5). Six healthy subjects with no history of neuromuscular disease served as controls. Informed consent was obtained from the patients and control subjects enrolled in the present study. The local ethics committee at Uppsala University Hospital approved the protocol and the experiments were carried out according to the guidelines of the Declaration of Helsinki.

Muscle Biopsies and Muscle Fiber Membrane Permeabilization. Fresh muscle biopsy specimens were obtained from the tibialis anterior and the vastus lateralis muscles under local anesthesia and placed in relaxing solution at 4 °C. Bundles of ≈50 fibers were dissected free and tied with surgical silk to glass capillary tubes at slightly stretched lengths. They were then treated with skinning solution (relaxing solution containing glycerol; 50:50 vol/vol) for 24 h at 4 °C, after which they were transferred to −20 °C. In addition, the muscle bundles were treated with sucrose, a cryoprotectant, within 1 to 2 weeks for long-term storage (30). They were detached from the capillary tubes and snap-frozen in liquid nitrogen-chilled propane and stored at −160 °C.

X-Ray Experimental Set-Up. Two to 3 days before X-ray recordings, fiber bundles were desucrosed and transferred to a relaxing solution, and single fibers were dissected. Arrays of ≈30 fibers were set up (17, 18, 29, 31). Both ends of each fiber were clamped to half-split gold meshes for electron microscopy (width, 3 mm), which had been glued to precision-machined ceramic chips (width, 3 mm) designed to fit to a specimen chamber. The arrays were then transferred to the skinning solution and stored at −20 °C.

On the day of X-ray recordings, arrays were placed in a plastic dish containing a preactivating solution and washed thoroughly to remove the glycerol. They were then transferred to the specimen chamber capable of manual length adjustment and force measurement (force transducer, AE801, Memscap). The specimen chamber was also filled with the preactivating solution. The mean sarcomere length was measured and set to 2.70 μm or > 3.60 μm. Subsequently, for arrays at a sarcomere length equal to 2.70 μm, optimal for humans (32), X-ray diffraction patterns were recorded at 15 °C, first in the preactivating solution and then in the activating solution when maximal steady-state isometric force was reached. It should be mentioned that the activating solution was supplied to the chamber by using a remote-controlled pump. For arrays at a sarcomere length > 3.60 μm, the protocol was identical except that preactivating and activating solutions were replaced by low-EGTA rigor and calcium-rigor solutions with 2,3-butanedione monoxime (to prevent occurrence of major sarcomere inhomogeneities).

X-Ray Diffraction Recordings and Analyses. For each array, ≈20 to 30 diffraction patterns (exposure time, 2 s) were recorded for each solution at the BL45XU beamline of SPring-8 and analyzed as described previously (17, 18, 29, 31). A total of 38 arrays (≈1,140 mounted fibers) were used. The wavelength was 0.09 nm and the specimen-to-detector distance was 2 m. As a detector, a cooled

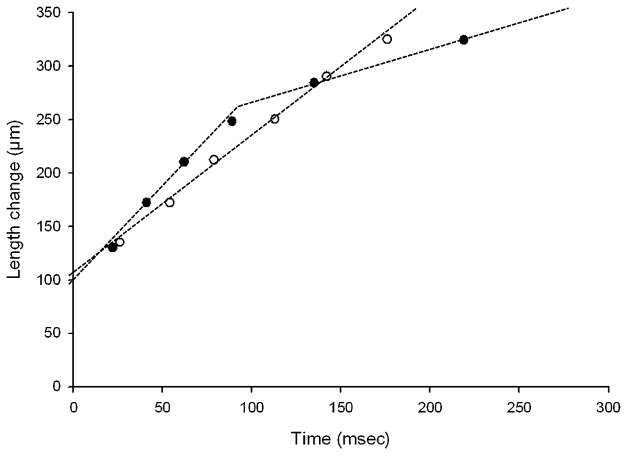

Fig. 4. Representative plots of slack-test procedure in a control fiber (○) and a mutated cell (●). Lengths were 1,620 and 1,700 μm, respectively.

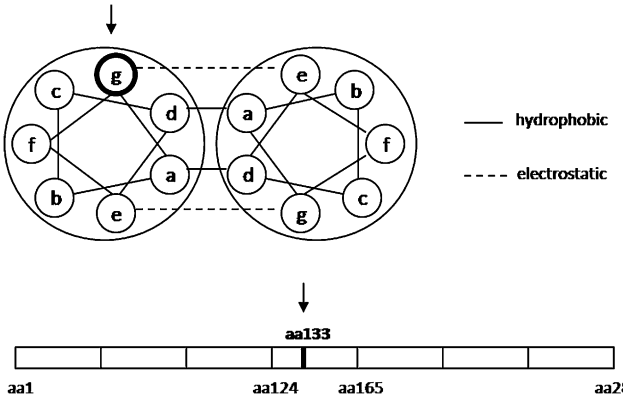

Fig. 5. Location (arrows) of the mutation in the heptad repeat and along the seven pseudorepeats of tropomyosin.

CCD camera (C4880, Hamamatsu Photonics; 1,000 × 1,018 pixels) was used in combination with an image intensifier (VP5445, Hamamatsu Photonics). To reduce radiation damage, we placed an aluminum plate (thickness 0.35–0.5 mm) upstream of the specimen chamber. The beam flux was estimated to be between 2.7×10^{11} and 4.0×10^{11} photons per second after attenuation, and the beam size at the sample position was 0.2 mm (vertical) and 0.3 mm (horizontal). Following X-ray recordings, background scattering was subtracted, and reflection intensities were determined as described elsewhere (9, 17, 18, 29, 31).

Slack-Test Procedure. On the day of the experiment, fiber bundles were desucrosed and transferred to a relaxing solution, and single fibers were dissected. A fiber 1 to 2 mm long was left between connectors leading to a force transducer (model 400A; Aurora Scientific) and a lever arm system (model 308B, Aurora Scientific) (33, 34). The apparatus was mounted on the stage of an inverted microscope (model IX70; Olympus). The sarcomere length was set to 2.70 to 2.80 μm and checked during the experiment with the use of a high-speed video-analysis system (model 901A HVSL; Aurora Scientific). In the activating solution, when maximal steady-state isometric force was reached seven releases of various amplitudes were rapidly introduced (within 1–2 ms) at one end of the fiber (35). Releases were applied at different amplitudes ranging from 7 to 17% of the fiber length. The fiber was re-extended between releases while relaxed to minimize changes in sarcomere length. During the slack-test, the time required to take up the imposed release was measured from the onset of the length step to the beginning of the tension redevelopment. A total of 17 fibers (eight controls and nine carrying the mutation) expressing the type I myosin heavy-chain isoform were included. It should be noted that for determining myosin heavy-chain isoform 6% SDS/PAGE gels were used as previously described (34). Briefly, the acrylamide concentration was 4% (wt/vol) in the stacking gel and 6% in the running gel, and the gel matrix included 30% glycerol. Sample loads were kept small (equivalent to ≈0.05 mm of fiber segment) to improve the resolution of the myosin heavy-chain bands (types I, IIa, and IIx). Electrophoresis was performed at 120 V for 24 h with a Tris-glycine electrode buffer (pH 8.3) at 15 °C (SE 600 vertical slab gel unit; Hoefer Scientific Instruments). The gels were silver-stained and subsequently scanned in a soft laser densitometer (Molecular Dynamics) with a high spatial resolution (50-μm pixel spacing) and 4,096 optical density levels.

Solutions. Relaxing and activating solutions contained (in mM) 4 Mg-ATP, 1 free Mg^{2+}, 20 imidazole, 7 EGTA, 14.5 creatine phosphate, 324 U/mL creatine phosphokinase, 1,000 U/mL catalase, and KCl to adjust the ionic strength to 180 mM and pH to 7.0. DTT (DTT) was also added. The preactivating solution was identical to the relaxing solution except that the EGTA concentration was reduced to 0.5 mM. The concentrations of free Ca^{2+} were 10^{-9} M (relaxing and preactivating solutions) and $10^{-4.5}$ M (activating solution). Low-EGTA rigor and calcium-rigor solutions, for overstretch experiments, had similar compositions to preactivating and activating solutions, except that MgATP, creatine phosphate, and creatine phosphokinase were absent, and that 2,3-butanedione monoxime was included with a concentration of 20 mM.

Statistical Analysis. Data are presented as means ± SE. Sigma Stat software was used to generate descriptive statistics. For sarcomere lengths of 2.70 μm and > 3.60 μm, two-way ANOVAs [group (control – R133W) × exposure (preactivation – activation)] were applied. In the event of differences, the post hoc Tukey test was performed. The level of significance was set at $P < 0.05$.

ACKNOWLEDGMENTS. We thank Dr. Eva Kimber for contacting the patients and Yvette Hedström for excellent technical assistance. This study was supported by grants from the Swedish Research Council, Association Française contre les Myopathies, the Tore Nilson Foundation, Apotekare Hedbergs Fund for Medical Research, a Human Frontier Science Program short-term fellowship, the Rector's travelling fellowship from the Wallenberg Foundation (to J.O.), and grants from the Swedish Research Council (8651), Association Française contre les Myopathies, the Swedish Cancer Foundation, European Commission (MyoAge, Fp7 CT-223756), King Gustaf V and Queen Victoria's Foundation, and the Thuréus Foundation (to L.L.). The experiments were performed under approval of the SPring-8 Proposal Review Committee (2008B1972 and 2009B1918).

1. Perry SV (2001) Vertebrate tropomyosin: Distribution, properties and function. *J Muscle Res Cell Motil* 22:5–49.
2. Lees-Miller JP, Helfman DM (1991) The molecular basis for tropomyosin isoform diversity. *Bioessays* 13:429–437.
3. Ochala J (2008) Thin filament proteins mutations associated with skeletal myopathies: Defective regulation of muscle contraction. *J Mol Med* 86:1197–1204.
4. Tajsharghi H, Kimber E, Holmgren D, Tulinius M, Oldfors A (2007) Distal arthrogryposis and muscle weakness associated with a beta-tropomyosin mutation. *Neurology* 68: 772–775.
5. Ochala J, et al. (2007) Effects of a R133W beta-tropomyosin mutation on regulation of muscle contraction in single human muscle fibres. *J Physiol* 581:1283–1292.
6. Lehman W, Craig R (2008) Tropomyosin and the steric mechanism of muscle regulation. *Adv Exp Med Biol* 644:95–109.
7. Huxley HE (1973) Structural changes in the actin- and myosin-containing filaments during contraction. *Cold Spring Harb Symp Quant Biol* 37:361–376.
8. Matsuo T, Yagi N (2008) Structural changes in the muscle thin filament during contractions caused by single and double electrical pulses. *J Mol Biol* 383:1019–1036.
9. Yagi N (2003) An X-ray diffraction study on early structural changes in skeletal muscle contraction. *Biophys J* 84:1093–1102.
10. Tamura T, Wakayama J, Inoue K, Yagi N, Iwamoto H (2009) Dynamics of thin-filament activation in rabbit skeletal muscle fibers examined by time-resolved X-ray diffraction. *Biophys J* 96:1045–1055.
11. Yagi N, Matsubara I (1989) Structural changes in the thin filament during activation studied by x-ray diffraction of highly stretched skeletal muscle. *J Mol Biol* 208:359–363.
12. Piazzesi G, et al. (2002) Mechanism of force generation by myosin heads in skeletal muscle. *Nature* 415:659–662.
13. Moss RL (1986) Effects on shortening velocity of rabbit skeletal muscle due to variations in the level of thin-filament activation. *J Physiol* 377:487–505.
14. Morris CA, Tobacman LS, Homsher E (2003) Thin filament activation and unloaded shortening velocity of rabbit skinned muscle fibres. *J Physiol* 550:205–215.
15. Martyn DA, et al. (1994) Unloaded shortening of skinned muscle fibers from rabbit activated with and without Ca2+. *Biophys J* 67:1984–1993.
16. Parry DA, Squire JM (1973) Structural role of tropomyosin in muscle regulation: Analysis of the X-ray diffraction patterns from relaxed and contracting muscles. *J Mol Biol* 75:33–55.
17. Iwamoto H, Oiwa K, Suzuki T, Fujisawa T (2002) States of thin filament regulatory proteins as revealed by combined cross-linking/x-ray diffraction techniques. *J Mol Biol* 317:707–720.
18. Iwamoto H (2009) Evidence for unique structural change of thin filaments upon calcium activation of insect flight muscle. *J Mol Biol* 390:99–111.
19. McLachlan AD, Stewart M (1975) Tropomyosin coiled-coil interactions: Evidence for an unstaggered structure. *J Mol Biol* 98:293–304.
20. Kohn WD, Mant CT, Hodges RS (1997) Alpha-helical protein assembly motifs. *J Biol Chem* 272:2583–2586.
21. Hitchcock-DeGregori SE, Song Y, Greenfield NJ (2002) Functions of tropomyosin's periodic repeats. *Biochemistry* 41:15036–15044.
22. Korman VL, et al. (2000) An actin subdomain 2 mutation that impairs thin filament regulation by troponin and tropomyosin. *J Biol Chem* 275:22470–22478.
23. Korman VL, Tobacman LS (1999) Mutations in actin subdomain 3 that impair thin filament regulation by troponin and tropomyosin. *J Biol Chem* 274:22191–22196.
24. Brown JH, et al. (2001) Deciphering the design of the tropomyosin molecule. *Proc Natl Acad Sci USA* 98:8496–8501.
25. Singh A, Hitchcock-DeGregori SE (2003) Local destabilization of the tropomyosin coiled coil gives the molecular flexibility required for actin binding. *Biochemistry* 42:14114–14121.
26. Singh A, Hitchcock-DeGregori SE (2006) Dual requirement for flexibility and specificity for binding of the coiled-coil tropomyosin to its target, actin. *Structure* 14:43–50.
27. Iwamoto H (1998) Thin filament cooperativity as a major determinant of shortening velocity in skeletal muscle fibers. *Biophys J* 74:1452–1464.
28. Yagi N, Matsubara I (1988) Changes in the 5.9 nm actin layer-line on activation of frog skeletal muscles. *Adv Exp Med Biol* 226:369–380.

29. Iwamoto H, Wakayama J, Fujisawa T, Yagi N (2003) Static and dynamic X-ray diffraction recordings from living mammalian and amphibian skeletal muscles. *Biophys J* 85:2492–2506.
30. Frontera WR, Larsson L (1997) Contractile studies of single human skeletal muscle fibers: A comparison of different muscles, permeabilization procedures, and storage techniques. *Muscle Nerve* 20:948–952.
31. Iwamoto H, Oiwa K, Suzuki T, Fujisawa T (2001) X-ray diffraction evidence for the lack of stereospecific protein interactions in highly activated actomyosin complex. *J Mol Biol* 305:863–874.
32. Ottenheijm CA, et al. (2009) Thin filament length dysregulation contributes to muscle weakness in nemaline myopathy patients with nebulin deficiency. *Hum Mol Genet* 18: 2359–2369.
33. Moss RL (1979) Sarcomere length-tension relations of frog skinned muscle fibres during calcium activation at short lengths. *J Physiol* 292:177–192.
34. Larsson L, Moss RL (1993) Maximum velocity of shortening in relation to myosin isoform composition in single fibres from human skeletal muscles. *J Physiol* 472:595–614.
35. Edman KA (1979) The velocity of unloaded shortening and its relation to sarcomere length and isometric force in vertebrate muscle fibres. *J Physiol* 291:143–159.